Clay minerals in the Meuse - Haute Marne underground laboratory (France): Possible influence of organic matter on clay mineral evolution.

Francis Claret, Boris A. Sakharov, Victor A. Drits, Bruce Velde, Alain Meunier, Lise Griffault, Bruno Lanson

Clay minerals in the Meuse - Haute Marne underground laboratory (France):

Possible influence of organic matter on clay mineral evolution

Francis Claret[1,2,*], Boris A. Sakharov[3], Victor A. Drits[3], Bruce Velde[4], Alain Meunier[5], Lise Griffault[2], Bruno Lanson[1]

1   Environmental Geochemistry Group, LGIT - Maison des Géosciences, University J. Fourier – CNRS, BP 53, 38041 Grenoble cedex 9, France

2   ANDRA, Parc de Croix Blanche, 1-7 rue Jean Monnet, 92298 Châtenay-Malabry Cedex, France

3   Geological Institute, Russian Academy of Sciences, 7 Pyzhevsky street, 119017 Moscow, Russia

4   Laboratoire de Géologie, Ecole Normale Supérieure - CNRS, 24 rue Lhomond, 75231 Paris cedex 5, France

5   Laboratoire HYDRASA, University of Poitiers - CNRS, 40 avenue du Recteur Pineau, 86022 Poitiers Cedex, France

[*]Corresponding author: claret@ine.fzk.de – Present address: Institut für Nukleare Entsorgung, FZK-INE, Postfach 3640, D-76021 Karlsruhe, Germany

Key words: Callovo-Oxfordian, Clay minerals, Clay diagenesis, Illite-smectite, Mixed-layering, interstratification, XRD, Organic matter, French underground laboratory, MHM site.

Clays & Clay Minerals Ms #848 – Revised version

ABSTRACT

A clay-rich Callovo-Oxfordian sedimentary formation was selected in the eastern Paris Basin (MHM site) to host an underground laboratory dedicated to the assessment of nuclear waste disposal feasibility in deep geological formations. As described initially, this formation shows a mineralogical transition from an illite-smectite (I-S) mixed-layered mineral (MLM), which is essentially smectitic and randomly interstratified (R=0) in the top part of the series to a more illitic, ordered (R≥1) I-S in its deeper part.

This description has been challenged by using the multi-specimen method developed by Drits *et al.* (1997a) and Sakharov *et al.* (1999). It is shown that all samples contain a physical mixture of an unusually (?) illitic (~65 %I) randomly interstratified I-Exp (Illite-Expandable MLM) and of a discrete smectite, in addition to discrete illite, kaolinite and chlorite. Structural parameters of the different clay phases vary little throughout the series. According to the proposed model, the mineralogical transition corresponds to the disappearance of smectite with increasing burial depth.

Comparison with clay minerals from formations of similar age (Oxfordian-Toarcian) throughout the Paris basin shows that the clay mineralogy in the deeper part of the series originates from a smectite-to-illite transition resulting from a low-temperature burial diagenesis. The anomalous lack of evolution of clay minerals in the upper part of the series is thought to be related to specific interactions between organic matter and clay minerals.

INTRODUCTION

As is the case for many other countries, France is investigating the possibility of nuclear waste disposal in deep geological formations. For this purpose, the French nuclear agency (ANDRA) is currently setting up an underground laboratory in the eastern Paris Basin, at the limit between the Meuse and Haute-Marne departments (MHM site - Figure 1). The sedimentary host formation is a ~130 m thick clay-rich Callovo-Oxfordian sedimentary formation whose burial depth is about 350-550 m below the ground surface in the selected area. The mineralogy of this formation was studied in detail by Bouchet and Rassineux (1997) and consists mainly of clay minerals, quartz and calcite.

These authors have shown that in spite of its macroscopic homogeneity, the Callovo-Oxfordian clay series conceals a mineralogical transition between two illite-smectite (I-S) mixed-layered minerals (MLMs). The first one occurs in the top part of the series and is essentially smectitic and randomly interstratified (R=0) whereas the deeper part of the series is characterized by a more illitic, ordered (R≥1) I-S. This mineralogical transition is reminiscent of the diagenetic smectite-to-illite evolution through MLMs commonly described during burial of clay-rich sediments (Burst, 1969; Shutov *et al.*, 1970; Perry and Hower, 1970; Hower *et al.,* 1976; Srodon, 1978, 1984; Boles and Francks, 1979; Velde *et al.,* 1986; among others). In these latter series, it has been deduced that time and temperature promote smectite illitization (Hower *et al.,* 1976; Velde and Vasseur, 1992), but additional factors such as K availability (Huang et *al*., 1993; Bauer and Velde, 1999) and water/rock ratio (Whitney, 1990) may also influence reaction progress.

In the studied Callovo-Oxfordian formation, the analysis of organic matter evolution (Elie *et al.,* 2000), and of fluid inclusions (Cathelineau *et al., 1997*) consistently indicate that maximum temperature has not exceeded 40°C. This low temperature together with the very

sudden character of the mineralogical transition, which occurs over a 10 m depth interval, and its coincidence at a local scale with a maximum flooding surface seem to plead for a sedimentary origin to this transition (Pellenard *et al.,* 1999), thus excluding any significant mineralogical evolution resulting from subsequent burial diagenesis. However, because the future underground laboratory will lie exactly in the mineralogical transition zone, additional investigations were performed in order to characterize the clay minerals from this transition zone more accurately in an attempt to better predict their possible evolution in response to storage-induced perturbations (Claret *et al.,* 2002) and possibly to reconsider the origin of the transition.

In this work, simulation of the experimental X-ray diffraction (XRD) patterns has been applied following the multi-specimen method proposed by Sakharov *et al.* (1999) to provide an accurate structural characterization of the clay minerals over the R0-R1 transition previously described in this Callovo-Oxfordian series. Clay minerals defining this transition are compared to those coming from formations of similar age (Oxfordian-Toarcian) throughout the Paris basin in order to assess the influence of low-temperature burial diagenesis on clay mineralogy. Finally the origin of the mineralogical transition is sought in the light of the strong interactions between organic matter and clay minerals demonstrated experimentally by Claret *et al.* (2002).

MATERIALS AND METHODS

Sample location and existing data

The boreholes sampled (EST 104 and EST 204) were drilled in the Callovo-Oxfordian formation selected by Andra to host the future French underground laboratory in the MHM

site. The selection of this macroscopically homogeneous clay-rich formation (152-160 Ma) results from its potential ability to impede any possible migration of radionuclides from the storage to the environment by combining a very low hydraulic conductivity (10^{-11}-10^{-13} m.s^{-1} - de Marsily *et al.*, 2002) to a large vertical extension ($\geq$ 40 m) on either side of the planned laboratory level.

From XRD data, bulk rock chemical composition and cation exchange capacity (CEC) measurements, Bouchet and Rassineux (1997) made a semi-quantitative estimate of the mineralogy throughout the Callovo-Oxfordian sequence. They determined that quartz and calcite were present in similar proportions and globally represented approximately 50% of the bulk rock, whereas clay minerals represented 40-45%. Minor amounts of accessory pyrite, hematite and siderite were also detected throughout the sequence. In well EST 104, the transition from randomly interstratified (R=0) to ordered (R=1) I-S MLMs described by Bouchet and Rassineux (1997) occurs within the 484-496 m burial depth interval. This transition correlates with a decrease of the CEC measured on the <2 µm size fraction from 0.35-0.40 meq.g^{-1} in the upper part of the sequence to ~0.25 meq.g^{-1} in its bottom part. In addition, this mineralogical transition coincides with the onset of kaolinite presence in the deeper sediments, whereas illite and minor amounts of chlorite are present throughout the sequence.

Even though present in small amounts (0.5-1%) organic matter (OM) occurs throughout the sequence (Espitalié *et al.,* 1987; Landais and Elie, 1999) and is systematically only slightly affected by thermal maturation, indicating a maximum burial temperature of ~40°C (Elie *et al.,* 2000). A similar low value of the maximum burial temperature has been obtained from the analysis of fluid inclusions (Cathelineau *et al.,* 1997). These values are consistent with the regional geological setting which indicates little post-sedimentation uplift and erosion during the Tertiary (Meunier and Velde, 2004). In the studied sequence, the nature of

the OM varies with burial depth, being from continental origin in the top part of the series (Oxfordian) but showing a stronger marine influence in its bottom part (Landais and Elie, 1999). However, these latter authors have shown that in the MHM site the transition between the two types of OM does not strictly coincide with the mineralogical transition, which is actually slightly shallower.

Additional samples were collected throughout the Paris basin to serve as a basis for comparing clay mineralogy in neighboring clay-rich formations. Four samples were collected in the few clay-rich Oxfordian horizons in the well EST 204 (MHM site – 218-250 m burial depth interval – 140-150 Ma). Other samples which were collected in the Toarcian black shales (180-190 Ma) from boreholes scattered throughout the Paris basin (Figure 1) were used to assess the influence of maximum burial depth on the low-temperature diagenetic evolution of clay minerals. The present burial depth of these samples which ranges from ~200 m in the eastern part of the Paris basin to ~2000 m in its central part is strictly correlated to their maximum burial depth which is a few hundred meters deeper throughout the basin as a result of a limited uplift and erosion event during the Tertiary (Lanson, 1990; Meunier and Velde, 2004).

Experimental

Carbonates were removed for all EST 104 and EST 204 samples using the acetic acid-acetate buffer method described in Moore and Reynolds (1989) prior to extraction of the <2 µm size fraction by centrifugation. Organic matter was removed at 50°C by adding small aliquots of hydrogen peroxide (H_2O_2 - 30%) to the suspension until gaseous emission has ceased. Size fractionation was used first on 29 samples selected from -417 to -528 m in borehole EST 104. From preliminary XRD results (Claret, 2001), 6 samples were selected as

being representative of the Callovo-Oxfordian series and more especially of the mineralogical transition (Figure 2). To minimize the contributions from mica, kaolinite, chlorite and quartz <0.2 µm size fractions were extracted for these 6 samples.

This <0.2 µm size fraction was then Ca-saturated with 1M $CaCl_2$. Suspensions were kept in contact with the saline solution for 4-12 hours at room temperature to ensure a complete cation exchange. After three replications of this procedure, the chloride in excess was rinsed out using distilled water (Milli-Q – 18.2 $M\Omega.cm^{-1}$) until no precipitate formed with $AgNO_3$. Samples from Toarcian black shales were prepared according to the method described by Lanson and Besson (1992)

Oriented preparations were obtained for XRD analysis by pipetting a slurry of the Ca-saturated suspensions on a glass side and drying at 40°C for a few hours to obtain an air-dried (AD) preparation. Ethylene glycol (EG) solvation of these oriented slides was achieved by exposing them to EG vapor at 70°C for 12 hours. XRD patterns of samples from EST 104 and EST 204 boreholes were recorded with a Bruker D5000 powder diffractometer equipped with a Kevex Si(Li) solid state detector using $CuK\alpha_{1+2}$ radiation. Intensities were recorded at a 0.04° 2θ interval, from 2 to 50°, using a 6 sec counting time per step. Sizes of the divergence slit, the two Soller slits, the antiscatter, and resolution slits were 0.5°, 2.3°, 2.3°, 0.5° and 0.06°, respectively. Using an Anton Paar TTK 450 chamber together with a Sycos H gas humidifier from Ansyco humidity was controlled at 40% RH for AD measurements. XRD data collection conditions for samples from Toarcian black shales were described earlier by Lanson and Besson (1992).

Clay particle morphology was characterized by TEM on the <0.05 µm size fraction to avoid as much as possible kaolinite, chlorite and detrital mica particles. Highly diluted suspensions were ultrasonically dispersed and subsequently deposited on carbon-coated

copper grids. Observations were made using a JEOL 100CX TEM with an accelerating voltage of 80 kV.

XRD profile modeling

Structure models were determined for the 6 clay samples selected from EST 104 using the multi-specimen method (Sakharov *et al.,* 1999). This method allows drawing constrains on the MLMs present in a given sample from the contrasting hydration/expansion properties of expandable interlayers after different treatments (e.g. Ca-saturated in AD and EG states, and/or Na-saturated in AD and EG states). The method itself consists of comparing directly experimental XRD profiles to those calculated from a structure model, the optimum fit to the experimental data being obtained by a trial-and-error procedure. Such structure models include for each MLM, the number (not limited to 2), the nature and the proportion of the different layer types and a statistical description of their stacking sequences (Reichweit parameter and junction probabilities - see Moore and Reynolds (1989) and Drits and Tchoubar (1990) for details). Because the different treatments may change the thickness and the scattering power of swelling interlayers but not the distribution of the different 2:1 layers, a consistent structure model is obtained when the stacking sequences of these different layer types are nearly identical for all experimental XRD profiles of the same sample. In addition to these structural parameters, relative contributions of the various phases to the different XRD patterns recorded for the same sample must be similar (Sakharov *et al.,* 1999; Claret, 2001).

The program developed by Drits *et al.* (1997a) and Sakharov *et al.* (1999) was used to fit experimental XRD profiles over the 2–50° 2θ CuKα range. Instrumental and experimental factors such as horizontal and vertical beam divergences, goniometer radius, length and thickness of the oriented slides were introduced without further adjustment (Drits and

8

Tchoubar, 1990). Sigmastar was set to 12 and the mass absorption coefficient (μ^*) to 45, as recommended by Moore and Reynolds (1989). In the profile fitting process, it was necessary to define three different layer types as a function of their hydration properties. In addition to illite layers, expandable layers were differentiated as smectite or vermiculite as a function of the number of EG sheets in their interlayers in the EG state (2 and 1, respectively – Drits *et al.,* 2002). Even though it does not coincide with the conventional nomenclature, this operational definition allowed accounting for the heterogeneous hydration/expansion behavior of expandable layers which is likely related to the amount and location of the layer charge. For the studied samples, it seemed unrealistic to assess otherwise the possible coexistence of layers with contrasting layer charge because of their polyphasic character. For these three layer types, hereafter referred to as I, S and V layers, z atomic coordinates and thermal displacement parameters (B) proposed by Moore and Reynolds (1989) were used for simulation. Position and amount of interlayer species (H_2O and EG molecules in particular) were considered as variable parameters during the fitting process and varied about the values proposed by Moore and Reynolds (1989) after modification of layer thickness (L. Tck.) values. As relative humidity was set to 40% during XRD data collection, it is assumed that no collapsed expandable layers are contributing to the relative proportion of illite layer. However, because the hydration properties of a given layer may vary as a function of the interlayer cation, relative proportions of vermiculite and smectite may vary for the different states of the samples. Finally, lognormal distributions of coherent scattering domain sizes (CSDS) were assumed and characterized by their mean value (Drits *et al.,* 1997b). Goodness of fit was estimated over the 4-50°2θ Cu Kα angular range using the R_{WP} factor (Howard and Preston, 1989).

RESULTS

Qualitative description of experimental XRD profiles

MHM site. Experimental XRD patterns can be divided in two groups. Following EG solvation, samples from group 1 (samples from 447, 482, 489, 492 and 494 m) exhibit a reflection at ~17 Å whose intensity above the low angle "background" decreases with increasing depth (Figure 2). According to Srodon (1981) and Inoue *et al.* (1989) such behavior is characteristic of a randomly interstratified I-S (R=0) whose smectite content decreases. From the diagram proposed by Inoue *et al.* (1989), the estimated proportion of smectite varies from ~70% at the top of the series and ~50% for sample 494.

Sample 528 does not show this 17 Å peak in its EG diffraction profile but rather a shoulder in the ~13.5 Å region corresponding to the ~12.5 Å hump observed in its AD pattern (Figure 2). The presence of these reflections is usually (Srodon, 1980; Watanabe, 1981, 1988; Velde *et al.,* 1986) linked to the presence of an ordered I-S (R=1) with a maximum possible degree of ordering (MPDO). From the diagram proposed by Velde *et al.* (1986) the smectite proportion in this MLM ranges from 20-40%.

Samples collected in the Oxfordian horizons from EST 204 borehole exhibit XRD patterns similar to those obtained from the deeper samples of the Callovo-Oxfordian series (Sample 528 - Figure 3a) and would usually be described as being characteristic of the presence of an ordered I-S (R=1). On the other hand, these XRD patterns are strikingly different from those obtained from the upper part of the Callovo-Oxfordian series which rather correspond to randomly interstratified (R=0) I-S MLMs (Group 1 samples - Figure 3a).

Additional samples from the Paris Basin.

All samples from Toarcian black shales collected throughout the Paris basin exhibit rather similar XRD patterns whatever their maximum burial depth (Figure 3b). These patterns resemble those obtained from the deepest Callovo-Oxfordian samples (MHM site - Sample 528). The presence of a ~12.5 Å reflection in the EG state, which correspond to the ~11.5 Å reflection in the AD state (Figure 3b), would usually be indicative of the presence of an ordered I-S MLM (R = 1) in addition to discrete illite, chlorite and kaolinite. The position of this reflection is rather constant indicating that the composition of the MLM is similar for all Toarcian samples whatever their maximum burial depth. As compared to the position observed for Callovian and Oxfordian samples (Figure 3a), this position is slightly shifted towards higher angles, indicating a slightly more illitic composition of the associated I-S MLMs.

Quantitative description of experimental XRD profiles

At first, XRD patterns of samples from group 1 were calculated for I-S compositions determined using the identification methods proposed by Srodon (1981) and Inoue *et al.* (1989). The results obtained using either of these methods differ significantly (Table 1) but none of these methods can provide a satisfactory fit to the experimental data as shown by the R_{WP} factors obtained after a least-square refinement of the relative contributions of the different phases (I-S, illite, ± kaolinite, ± chlorite) to the diffracted intensity. As a consequence, the multi-specimen method developed by Drits *et al.* (1997a) and Sakharov *et al.* (1999) was used to obtain structure models for all samples from the Callovo-Oxfordian series (EST 104 borehole).

Contribution of individual minerals phases to XRD patterns. For samples of group 1, the optimum fit to the experimental data was obtained using a physical mixture of a randomly interstratified I-Exp (Illite-Expandable MLM) and of discrete smectite (Figure 4), in addition to discrete illite, kaolinite and chlorite. Optimum structural parameters of the different phases contributing to the diffracted intensity are listed in Tables 2a-c for Callovo-Oxfordian samples from EST 104 borehole (Figures 5, 6 and 7). These structural parameters vary little throughout the series (Tables 2a-c) thus justifying the use of the term "phase" to describe these different contributions. Relative proportions of these phases obtained for both AD and EG states are listed in Table 2d.

From Figure 4, it is clear that the ~17 Å maximum observed on the XRD patterns of the Callovo-Oxfordian samples and which was originally attributed to a randomly interstratified I-S, rather corresponds to the contribution of discrete smectite. As a consequence the steady decrease of this maximum with increasing depth is related to the decreasing proportion of smectite (Table 2d). In addition, one may note that the proportion of the discrete smectite is lower than that of the randomly interstratified I-Exp phase in spite of the very intense contribution of the former phase to the XRD pattern because of contrasting structure factors for the two phases. Because the structure factor is very high for the 001 reflection of EG-solvated smectite, it is possible to detect the contribution of this phase even if present in a very low proportion (1-4%) as in samples 492 or 494 (Figure 6). In the low angle region, the randomly interstratified I-Exp contributes only to an increased "background" without any significant intensity modulations (Figure 4). The contribution of this I-Exp phase increases slightly with increasing depth (Table 2d), whereas the relative proportion of illite is about constant throughout the whole Callovo-Oxfordian sequence.

Detailed composition of the different minerals contributing to XRD patterns. All samples from the Callovo-Oxfordian series sampled in the EST 104 borehole are a physical mixture of a randomly interstratified I-Exp and of discrete smectite in addition to discrete illite, kaolinite and chlorite (Figure 4). Discrete illite systematically contains a small amount of randomly interstratified expandable layers (~5%), and the non-expandable layers exhibit a constant interlayer composition with 0.95 K atoms per $O_{10}(OH)_2$. The mean coherent scattering domain size (CSDS) along the c* axis remains constant throughout the series for this discrete illite phase with 12 layers in both AD and EG states. Because of their overwhelming proportions in the samples (Table 2d) and because of their potential impact on the retention properties in the geological formation special attention will be paid to the mineralogical description of discrete smectite and of the randomly interstratified I-Exp phase.

The expandability with EG of discrete smectite is similar for all samples from Group 1 (Table 2a), with the systematic presence of 2 sheets of EG molecules and a basal spacing of 16.7 Å after EG solvation. In contrast, the hydration behavior of these expandable layers is heterogeneous with about one third of the expandable layers incorporating only one sheet of H_2O molecules after Ca-saturation. However, the ratio between these two layer types is constant throughout the series. In addition, the mean CSDS along the c* axis remains constant for this discrete smectite phase throughout the series with 3.5 and 3.0 layers in the AD and EG states, respectively.

The very illitic composition of the randomly interstratified I-Exp phase, although unusual in sedimentary series, is also very constant throughout the studied sequence, with only a slight increase of its illite content in sample 528 (from 65 to 70 %I - Tables 2b,c). The swelling behavior of the Ca-saturated expandable layers is similar all for group 1 samples (Table 2b) as about 70% of these layers incorporate 2 sheets of EG molecules after EG solvation to systematically exhibit a 17.0 Å basal distance (S layers). Only 1 sheet of EG

molecules is present in the remaining expandable layers leading to a basal distance of 12.9 Å (V layers). In the AD state, the hydration behavior of these expandable layers is also constant for group 1 samples with 60-70% of these layers hosting 2 sheets of H_2O molecules (L. Tck. = 15.0 Å), while the remaining layers accept only 1 sheet of H_2O molecules (L. Tck. = 12.5 Å). On the other hand the swelling behavior of these expandable layers is much more heterogeneous for sample 528 leading in particular to the description of this contribution as two MLMs having the same I:Exp ratio (70:30). The composition (I:Exp = 70:30) and the stacking sequence (R = 0) of the first MLM (MLM1 - Table 2c) is similar to that of the I-Exp phase in samples of group 1 (Table 2b). All expandable layers of this MLM1 incorporate 2 sheets of EG molecules after EG solvation (L. Tck. = 16.8 Å), whereas one third of these layers accept only 1 sheet of H_2O molecules associated with Ca^{2+} cations (L. Tck. = 12.5 Å) in the AD state. The swelling behavior of expandable layers present in the second MLM (MLM2) is more complex (Table 2c). After EG solvation, expandable layers with 1 and 2 sheets of EG molecules (L. Tck. = 13.5 Å and 16.8 Å, respectively) are present in equal proportions. In addition, the former layers are segregated (R = 1) as P_{VV} (0.40) is greater than the abundance of vermiculite layers (W_V = 0.15 - Table 2c). The hydration behavior of expandable layers in the AD state is even more complex leading to the description of the MLM2 contribution as two MLMs. In the first one, layers which fully expand after EG solvation (S layers), are randomly distributed between S and V1 layers (1:2 ratio) in the AD state ($W_{S-EG} = W_{S-AD} + W_{V1-AD}$), whereas V layers in the EG state remain only partially hydrated (V2 layers), exhibiting the same tendency to segregation ($P_{VV-EG} = P_{V2V2-AD} = 0.40 >$ W_{V2-AD}). In the second MLM, all layers which fully expand (S layers) after EG solvation incorporate two sheets of H_2O molecules in the AD state (S1 layers – $W_{S-EG} = W_{S1-AD}$), whereas V layers in the EG state are represented by S2 and V layers (1:2 ratio) in the AD state ($W_{V-EG} = W_{S2-AD} + W_{V-AD}$). Again, the tendency to segregation of these V layers is

maintanied in the AD state ($P_{S2S2-AD} > W_{V2-AD}$, and $P_{VV-AD} > W_{V-AD}$ – Table 2c) and the occurrence probability of VV pairs in the EG state ($W_{VV} = W_V$ x $P_{VV} = 0.06$) is kept constant in the AD state (W_{S2} x ($P_{S2S2} + P_{S2V}$) + W_V x ($P_{VS2} + P_{VV}$) = 0.06 – Table 2c).

However, if the contributions of MLM1 and MLM2 to the Ca-EG diffraction pattern are considered together, the occurrence probability of II, IS, … layer pairs is similar to that of a randomly interstratified I-Exp (70:30) MLM (Figure 8). The only significant difference is induced by the slight tendency to segregation of V-type layers.

To summarize, from group 1 to sample 528 samples the structural evolution of the I-Exp phase may be described as 1) an increased proportion of non-expandable layers, 2) a reduced ability of the expandable layers to incorporate 2 sheets of EG molecules after EG solvation possibly indicating a higher layer charge, and 3) a tendency to segregation of these V-type layers. In addition, one may note that the K-content of the I-type layers (0.75 K atoms per $O_{10}(OH)_2$) is lower than that obtained for the discrete illite phase.

Influence of structural parameters on calculated XRD patterns

During the trial-and error fitting of a simulated XRD pattern to the experimental data a large number of parameters are adjusted, and the relevance of the different "improvements" has to be assessed to validate the increased complexity (realism ?) of the proposed model. As the main parameters used to characterize a MLM are the number and nature (layer thickness but also chemical composition) of the different layer types, their relative proportions and junction probabilities, these parameters were specifically assessed.

The sensitivity to the number of different layer types in a given MLM was assessed first for sample 447 (Ca-EG) by assuming that all expandable layers in the I-Exp MLM are S-type layers incorporating 2 sheets of EG molecules after EG solvation leading to a 65:35:0 I:S:V

ratio as compared to the optimum 65:25:10 value (Table 2b). The resulting fit to the experimental data (Figure 9a) is of poorer quality (R_{WP} = 10.2% as compared to the optimum 8.8%). This modification leads in particular to the presence of a sharp maximum on the high angle side of the illite 001 peak (9.98 Å - Figure 9a) and to a significant intensity decrease of the high angle side of the illite 002 peak (5.00 Å). In addition, relative abundances of discrete smectite, I-Exp MLM and discrete illite (25, 45, and 30%, respectively) are different from the optimum values (25, 55, and 20%, respectively) leading to significant discrepancies with the values obtained on the Ca-AD XRD pattern (24, 54, and 21%, respectively).

The sensitivity to junction probabilities in a given MLM was assessed for sample 447 (Ca-EG) by assuming a slight segregation of S-type layers in the I-Exp MLM. In the calculated pattern P_{SS} was increased from the optimum 0.25 value ($P_{SS} = W_S$, as R = 0 - Table 2b) to 0.40, whereas all other independent parameters (P_{SV}, P_{VS} and P_{VV}) were kept constant (0.10, 0.25 and 0.10, respectively – Table 2b). Again, the quality of fit is significantly decreased (R_{WP} = 11.5% as compared to the optimum 8.8%) and significant discrepancies are visible (Figure 9b) on the low-angle side of the illite 001 peak (9.98 Å) and on the intensity of the 3.33 Å maximum.

The sensitivity to the nature of the different layer types is illustrated for sample 447 (Ca-EG) by assuming first that the basal distance of the minor S-type layers in the I-Exp MLM is decreased from the optimum 17.0 Å value to 16.7 Å as for discrete smectite. Even though the overall agreement with the experimental XRD pattern is similar to the optimum one (R_{WP} = 8.8% as for the optimum fit), a significant shift of the calculated 3.33 Å maximum as compared to the experimental XRD pattern is observed (Figure 9c) supporting the hypothesis of a L. Tck. value of 17.0 Å. The chemical composition, and more specifically the interlayer K content, may also be efficiently constrained because of its influence on the calculated XRD profiles. If, for example, the K-content of the I-type layers in the I-Exp MLM

is assumed to be 0.90 (K per $O_{10}(OH)_2$), instead of the optimum 0.75 value, the agreement between calculated and experimental patterns for sample 492 (Ca-EG) is significantly deteriorated (R_{WP} = 15.0% as compared to the optimum 10.1%). Specific discrepancies occur on peak intensity of the illite 001 peak and on the two sides of the illite 002 peak (9.98 Å and 5.00 Å, respectively - Figure 9d)

DISCUSSION

Validity of the proposed mineralogical description

Samples from group 1 may be described as containing, in addition to discrete illite, kaolinite and chlorite, a mixture of a discrete smectite and of a randomly interstratified I-S-V MLM (polyphasic model). An alternative model was also considered in which the smectite and I-Exp MLM contributions were combined into a unique I-S-V MLM showing a strong tendency to segregation (R = 1 – segregated model). Even though the two conceptual models are strikingly different (a monophase Vs. a physical mixture) the layer pair abundances (W_{ij}) calculated for the two models are similar and the diffraction effects obtained for both models are close. However, the first hypothesis has been preferred for several reasons which will be discussed hereafter. The first endorsement for this preference comes from the better quality of fit obtained using this model with two contributions. However, this improved quality of fit should be weighted against the increased number of adjustable parameters resulting from the split of the segregated I-S-V contribution in two independent contributions. No quantitative estimate has been made but this increase is basically limited to the possibility of having different CSDS for the two phases and different L. Tck. for the S-type layers in these phases, and in our opinion, cannot account alone for the improved quality of fit. Furthermore, the

polyphasic model allowed to meet the additional constrains coming from the relative proportions of the different phases determined from the analysis of different XRD patterns for the same sample (Claret, 2001). This model also allowed us to propose a consistent description of the clay mineralogy for all samples from the Callovo-Oxfordian series which contain a discrete smectite phase and a randomly interstratified I-Exp MLM (I:Exp ratio ≈ 2:1) in addition to discrete illite, kaolinite, and chlorite. Additional data supporting the polyphasic model comes from the high-pH alteration experiments performed by Claret *et al.* (2002) on the same Callovo-Oxfordian samples. These authors indeed showed, using sample 490, that the smectite phase is preferentially altered during these experiments, leading to the formation of a randomly interstratified I-Exp MLM (I:Exp ratio being 50:50 in this new phase), whereas the original I-Exp MLM is left unaltered. On the one hand, this behavior is consistent with the likely contrasting stabilities of discrete smectite and I-Exp MLM in these high pH conditions. For the segregated model on the other hand, this behavior implies the specific alteration of clusters of expandable layers in the segregated I-Exp, whereas isolated expandable layers in the same I-Exp phase would be left unaltered. Because we could not think of a rationale for the contrasting stability of similar expandable layers, the experiments performed by Claret *et al.* (2002) were assumed to support the polyphasic model.

Clay mineralogy in the Callovo-Oxfordian series

In the samples studied, the main clay phase is the randomly interstratified I-Exp MLM which accounts for about 60% of the diffracting material in the <0.2 μm size fraction. The very illitic composition of this MLM phase, which contains about 65% of non-expandable illite layers, is seldom described for I-S MLMs in diagenetic environments as interstratification is most often described as ordered (R = 1 with maximum possible degree of

18

ordering – MPDO ; see Drits and Tchoubar (1990) for details) for I-S MLMs in which illite prevails (Moore and Reynolds, 1989). However, the illite content in I-Exp MLMs corresponding to the R = 0 to R = 1 transition is not strictly defined in the literature. For example, from the analysis of the XRD results obtained on Gulf Coast samples by Perry and Hower (1970), Bethke *et al.* (1986) has set this transition between 60-70 %I for shales. Samples identified by Perry and Hower (1970) as containing such a highly illitic randomly interstratified MLM (E-10080, C-15509, e.g.) exhibit XRD patterns very similar to that of samples 492 and 494 in which the smectite contribution is faint. After EG solvation, these XRD patterns show only a broad and poorly defined shoulder at ~17 Å, and the contribution of such a highly illitic randomly interstratified MLM to the diffracted intensity is extremely diffuse (Figure 4). Because position of diffraction maxima is widely used to identify MLMs, this specific diffraction fingerprint, without any significant maximum, likely hinders the recognition of such highly illitic randomly interstratified MLMs in natural samples and is most likely responsible for their seldom described occurrence. Such highly illitic (60-70%Ill) randomly interstratified MLMs have also been recognized in soils (Righi *et al.*, 1995; Velde and Peck, 2002)

A peculiarity of this randomly interstratified I-Exp MLM comes from the composition of its I-type interlayers which contain 0.75 K atoms per $O_{10}(OH)_2$ according to XRD profile modeling. This low K-content, which is confirmed by the sensitivity tests (Figures 6a and 9d), is in agreement with early studies of Hower and Mowatt (1966) and Srodon and Eberl (1984). This low K-content is not associated with the presence of $NH4^+$ as interlayer cations as the basal distance determined from the simulation of XRD patterns for non-expandable layers is systematically 9.98 Å. If NH_4^+ cations were present (tobelite-like layers) this would lead to an increase of the d-spacings as described by Drits *et al.* (2002). However, this composition was challenged by Meunier and Velde (1989) who determined a higher layer charge (0.87 per

O$_{10}$(OH)$_2$) from the interpolation of published chemical data. This higher K-content in illite was later confirmed by Lanson and Champion (1991) from EDS analysis on a TEM, and by Srodon *et al.* (1992) from the combination of EDS analyses on TEM, and CEC and total surface measurements. One possible explanation for this discrepancy may lie in the nature of the samples analyzed in these latter studies as most chemical data do not come shales samples but rather from bentonites. This hypothesis is supported by the similar low K-content determined by Sakharov *et al.* (1999) for shale samples, in contrast with the higher K-contents they reported for hydrothermal and bentonite samples. Such low K-content of illite layers in shales has also been reported by Drits *et al.* (1997a, 2002), and Lindgreen *et al.* (2000) using a similar multi-specimen approach to XRD patterns. It should be noted that the K-content in the discrete illite phase is much higher (0.95 per O$_{10}$(OH)$_2$) than that in the I-Exp MLM.

Another essential feature of the expandable clay phases in the Callovo-Oxfordian samples is the heterogeneous hydration and swelling behaviors for expandable layers. This heterogeneity, which has been accounted for by using two types (S and V) of expandable layers with contrasting hydration./expansion properties, likely results from different amounts, and possibly location, of the layer charge. However, the binary (S- or V-type) hydration/expansion behavior of expandable layers is only a simplistic indication of their charge distribution which could be better assessed by using different interlayer cations and relative humidities (see for example Calarge et al., 2003 or Meunier et al., 2004) and/or alkylammonium cations. This heterogeneity has long been recognized in the AD state and, as a consequence, most identification methods for I-Exp MLMs are based on the analysis of XRD patterns recorded after EG solvation (Srodon 1980, 1981; Watanabe, 1981, 1988; Velde *et al.,* 1986; Inoue *et al.,* 1989). However, in our opinion this intrinsic heterogeneity is an indicator of the burial diagenesis evolution in particular for the early stages of smectite illitization, in which significant structural modifications of the expandable layers occur

without illite layer formation (Sato *et al.,* 1996; Drits *et al.*, 1997a; Beaufort *et al.,* 2001). In addition, even though in the discrete smectite all expandable layers incorporate two sheets of EG molecules after EG solvation, the swelling heterogeneity is preserved for the I-Exp MLM, which contains about one third of expandable layers with a unique sheet of EG molecules (Table 2b). Because of this swelling heterogeneity, which is very likely to be common (see Meunier *et al.* (2000) for a review), most usual identification methods for I-Exp MLMs are unable to provide a good description of natural samples as they are based on the assumption of two-component (I-S) MLMs.

Evolution of clay mineralogy in the Callovo-Oxfordian series

The data described in the present article offer a novel description of the "R0-to-R1" transition originally described by Bouchet and Rassineux (1997) in the Callovo-Oxfordian series of the MHM site. In the proposed description, the structural characteristics of the different contributions to the diffracted intensity are nearly constant throughout the series, thus justifying the use of the term "phase" to describe these different contributions. The CSDS and the I:Exp ratio are about constant for all these contributions, and the hydration/swelling behavior of expandable layers does not change significantly with depth. The main structural evolution occurs for sample 528, in which the contribution of the I-Exp MLM is split because of the increased heterogeneity of swelling properties in expandable layer. However, if the two contributions are considered together, they are very close to that of a randomly interstratified I-Exp containing 70% illite layers as shown by the calculated occurrence probabilities of the different layer pairs (Figure 8).

As a consequence, the mineralogical transition described by Bouchet and Rassineux (1997) does not correspond to the progressive illitization of I-S MLMs as originally proposed

but rather to the disappearance of smectite with increasing depth. In the new description, XRD patterns (after EG solvation) exhibiting a vague shoulder at ~17 Å are indicative of an illite-rich (~65 %I) randomly interstratified I-Exp MLM similar to the one originally described by Perry and Hower (1970) in deeply buried Texas Gulf Coast "R = 0" samples. In addition, in the present case study the progressive decrease of the 17 Å peak/low angle shoulder intensity ratio is not indicative of the increasing proportion of illite layers in a randomly interstratified I-S MLM, as assumed by Inoue *et al.* (1989) and by Bouchet and Rassineux (1997) for smectite-to-illite conversion series, but rather corresponds to the decreasing proportion of a discrete smectite phase. Claret (2001) has shown that the use of the multi-specimen method on clay-size fractions of samples from the Gulf Coast classic diagenetic smectite-to-illite conversion series leads to a similar mineralogical description for the uppermost part of the series in which randomly interstratified I-Exp MLMs dominate.

Evidence for a low-temperature mineral diagenesis

One objective of the present study was also to unravel the possible origin of the observed mineralogical transition, and more especially to assess the sedimentological control on this transition suggested by Pellenard *et al.* (1999). The clay mineralogy of the Callovo-Oxfordian series was thus compared to that of other formations of similar ages (Oxfordian – Toarcian) occurring in the Paris basin. From the qualitative comparison of XRD patterns, the mineralogy of these formations is akin to that of sample 528, whereas samples from group 1 exhibit strikingly different XRD patterns (Figure 3). One may note that sample 528 is similar to older Toarcian sediments collected throughout the Paris basin (Figure 3b) and to younger Oxfordian sediments sampled in the MHM site (Figure 3a). According to usual identification criteria (Velde *et al.,* 1986) I-S MLMs observed in sample 528 from the Callovo-Oxfordian

series and in Oxfordian samples would contain ~40% of expandable layers (I-Exp peak position at about 12.5 Å in the Ca-AD state - Figures 2 and 3a). Toarcian samples (180-190 Ma) exhibit a more illitic clay mineral composition, as compared to younger Oxfordian and Callovian samples (150-162 Ma), as indicated by the I-Exp peak position at about 11.5 Å in the Ca-AD state the position (Figure 3b). In addition, because XRD patterns of all Toarcian samples are alike whatever their maximum burial depth the driving force for the smectite-to-illite evolution is most likely time rather than temperature for these Jurassic sediments. All above observations suggest that the clay mineralogy of sample 528 is consistent with that described in formations of similar ages as resulting from a diagenetic smectite-to-illite transition.

The assumption of a pervasive low-temperature diagenesis is supported by the presence throughout the Callovo-Oxfordian series of clay-size particles exhibiting idiomorphic shapes (Figure 10) indicating a systematic crystallization of clay (I-Exp MLMs) particles. Similar neoformed particles have also been observed by Rousset and Clauer (2003) in the same formation. However, these authors plead for a limited clay diagenesis because radiogenic ages measured in the Callovo-Oxfordian sediments are systematically older than stratigraphic ages. This apparent contradiction is probably due to the systematic presence of discrete illite even in the finest size fractions. This phase, which is likely of detrital origin, accounts for about 25% of the <0.2 µm (Table 2d), and its high K-content may exert a strong influence on measured radiogenic ages.

From the comparison between kerogen maturation and I-S composition made by Velde and Espitalié (1989) for Jurassic samples (150-180 Ma) the I-S composition in sample 528 (20-40%S from the method developed by Velde et al (1986)) corresponds to the absence of any kerogen (type III) transformation, which is consistent with the very low maximum temperature recorded by OM (Elie *et al.,* 2000) and fluid inclusions (Cathelineau *et al.,* 1997).

On the other hand , the clay mineralogy of group 1 samples is noticeably different from sample 528 and the origin for their "immature" character in the general scheme of smectite illitization should be sought. In other words, the problem is not to understand the origin of the sudden transition from smectite-rich sediments to illite-rich sediments but rather to understand why in the upper part of the series the smectite-rich sediments have not evolved towards more illitic compositions.

Origin of the observed mineralogical transition

The above discussion has shown that the low maximum burial temperature experienced by these Callovo-Oxfordian sediments is not responsible for the absence of mineralogical evolution in the upper part of the series. Furthermore, the sudden character of the mineralogical transition, which occurs over a 10 m depth interval, results in an extremely low temperature difference between the two parts of the series that can not account for the observed contrast of their clay mineralogy. Similarly, the chemical homogeneity of the formation, which confers constant geochemical characteristics to the bulk rock and identical octahedral and interlayer compositions to the clay fraction throughout the Callovo-Oxfordian formation (MHM site – Rousset and Clauer, 2003), does not plead for a chemical origin to this mineralogical transition. Because the availability of K is known as a possible limiting factor for smectite illitization (Pytte and Reynolds, 1989; Whitney, 1992; Huang *et al.*, 1993), it was specifically checked that K-feldspars and detrital micas are present throughout the series as a potential K-source.

As the low-temperature and the K-availability hypotheses on the origin of the observed mineralogical transition can be ruled out, the very low degree of clay mineral diagenesis of the uppermost (group 1) samples can be alternatively connected to the low clay reactivity

evidenced on the same samples by Claret *et al.* (2002) in his high pH experiments. From these experiments, and more especially from X-ray microscopy observations, Claret *et al.* (2002) has shown that the organic coating on the edges of clay particles is responsible for a limited reactivity of clay minerals from the Callovo-Oxfordian series. Using in particular the steranes:hopanes and pristine:phytane ratios Landais and Elie (1999) have determined that the nature of this OM varies with burial depth in the MHM site, being from continental origin (type III) in the top part of the series (Oxfordian) whereas it shows stronger marine influence (type II) in its bottom part. It is therefore likely that the influence of OM on clay reactivity will be different in the upper and deeper parts of the series as a result of this contrasting origin and nature. In particular, OM may totally impede the reactivity of clay particles in the upper part of the series whereas the reactivity of clay minerals is only partly affected in the deeper part of the series. This is consistent with the results of Claret *et al.* (2002). These authors indeed observed strictly no evolution for their uppermost sample (447) whereas partial smectite dissolution was described for sample 490 under the same experimental conditions.

However, Landais and Elie (1999) have shown that the transition between the two types of OM does not strictly coincide with the mineralogical transition, which is actually slightly shallower in the MHM site. As a consequence these different OM inputs can not account alone for the mineralogical transition observed within the Callovo-Oxfordian series. On the other hand, these two primary continental and marine domains are not homogeneous as some of the OM geochemical parameters vary within these domains. Such variation of geochemical parameters may reflect subtle differences in the origin or in the evolution of OM after deposition (e.g. contrasting depositional environments) and could lead to contrasting reactivity of the OM. In turn, interactions between this OM and clay minerals may allow a "normal" low-temperature diagenetic smectite-to-illite evolution in the deeper part of the Callovo-Oxfordian series whereas they can considerably slow down the evolution of clay

minerals in the upper part of the series. For example, the change in the distribution of alkyl-napthalenes (Landais and Elie, 1999 – Figure 3.7), which occurs within the Oxfordian domain, coincides with the observed mineralogical at a burial and could possibly indicate such a difference of OM reactivity.

As a consequence, it seems likely that the origin of the observed mineralogical transition is actually related to sedimentology (Pellenard *et al.,* 1999). However this influence does not come from contrasting mineral contributions as supposed earlier (Pellenard *et al.,* 1999), but rather from different inputs of OM coming with these detrital mineral contributions or from different evolutions of this OM after deposition.

CONCLUSION

XRD patterns of the studied Callovo-Oxfordian series of samples are very similar to those described in the literature as characteristic of a diagenetic smectite-to-illite conversion series. However, for the studied series, the multi-specimen method leads to their description as a physical mixture of a seldom described illitic (~65 %I) randomly interstratified I-Exp (Illite-Expandable MLM) and of a discrete smectite, in addition to discrete illite, kaolinite and chlorite.

The mineralogical composition of the deepest sample is akin to that of clay-rich formations of similar age (Oxfordian-Toarcian) sampled throughout the Paris basin, thus pleading for a similar low-temperature burial diagenetic origin (smectite-to-illite transition). The anomalous lack of evolution of clay minerals in the upper part of the series is thought to be related to specific interactions between organic matter and clay minerals, even though the major change in OM origin is not strictly coincident with the mineralogical transition.

According to the proposed model, the mineralogical evolution observed in the top part of the series (group 1 samples) corresponds to the disappearance of smectite with increasing depth. The diffuse diffraction fingerprint of the highly illitic randomly interstratified MLM (mostly a broad hump in the low-angle region) is likely to be responsible for its scarce identification in natural samples.

The sensitivity of the multi-specimen method developed by Drits *et al.* (1997a) and Sakharov *et al.* (1999) to small structural variations has been strongly enhanced by the additional constraint imposed from the required coincidence between relative proportions of the different phases determined from the various XRD patterns recorded on the same sample. This constraint represents an additional criterion to select between different structure models leading to fits of similar quality to the experimental patterns.

REFERENCES

Bauer, A. and Velde, B. (1999) Smectite transformation in high molar KOH solutions. *Clay Minerals*, **34**, 259-273.

Beaufort, D., Berger, G., Lacharpagne, J. C. and Meunier, A. (2001) An experimental alteration of montmorillonite to a di+trioctahedral smectite assemblage at 100 and 200°C. *Clay Minerals*, **36**, 211-225.

Bethke, C. G., Vergo, N. and Altaner, S. P. (1986) Pathways of smectite illitization. *Clays and Clay Minerals*, **34**, 125-135.

Boles, J. R. and Francks, G. S. (1979) Clay diagenesis in Wilcox sandstones of Southwest Texas: Implications of smectite diagenesis on sandstone cementation. *Journal of Sedimentary Petrology*, **49**, 55-70.

Bouchet, A. and Rassineux, F. (1997) *Echantillons d'argiles du forage EST 104 : Etude minéralogique approfondie.* Andra, Report DR-P-0ERM-98-007A, Chatenay Malabry, France, 107 pp.

Burst, J. F. (1969) Diagenesis of Gulf Coast clayey sediments and its possible relation to petroleum migration. *American Association of Petroleum Geologists Bulletin*, **53**, 73-93.

Calarge, L., Lanson, B., Meunier, A., and Formoso, M.L. (2003) The smectitic minerals in a bentonite deposit from Melo (Uruguay). *Clay Minerals*, **38**, 25-34.

Cathelineau, M., Ayt Ougougdal, M., Elie, M. and Ruck, R. (1997) Mise en evidence d'une diagénèse de basse température dans les series mésozoiques du site Est : une étude des inclusions fluides des argiles et de la matière organique. *Proceeding of the Journées scientifiques, ANDRA, CNRS, Bar le duc*, pp. 28.

Claret, F. (2001) Caractérisation structurale des transitions minéralogiques dans les

    formations argileuses : Contrôles et implications géochimiques des processus

    d'illitisation. Cas particulier d'une perturbation alcaline dans le Callovo-Oxfordien

    Laboratoire souterrain Meuse-Haute-Marne. Ph.D. thesis, Université Joseph Fourrier,

    Grenoble, France, 174 pp.

Claret, F., Bauer, A., Schäfer, T., Griffault, L. and Lanson, B. (2002) Experimental

    investigation of the interaction of clays with high pH solutions : A case study from the

    Callovo-Oxfordian formation, Meuse-Haute Marne underground laboratory (France).

    Clays and Clays Minerals, **50**, 633-646.

Drits, V. A. and Sakharov, B. A. (1976). *X-Ray structure analysis of mixed-layer minerals*.

    Dokl. Akad. Nauk SSSR, Moscow, 256 pp.

Drits, V. A. and Tchoubar, C. (1990). *X-ray diffraction by disordered lamellar structures:*

    Theory and applications to microdivided silicates and carbons. Springer-Verlag,

    Berlin, 371 pp.

Drits, V. A., Lindgreen, H., Sakharov, B. A. and Salyn, A. S. (1997a) Sequence structure

    transformation of illite-smectite-vermiculite during diagenesis of Upper Jurassic

    shales, North Sea. *Clay Minerals*, **32**, 351-371.

Drits, V. A., Srodon, J. and Eberl, D. D. (1997b) XRD measurement of mean crystallite

    tickness of illite and illite/smectite : Reapparisal of the Kubler index and the scherrer

    equation. *Clays and Clays Minerals*, **45**, 461-475.

Drits, V. A., Lindgreen, H., Sakharov, B. A., Jakobsen, H. J., Salyn, A. L. and Dainyak, L. G.

    (2002) Tobelitization of smectite during oil generation in oil-source shales.

    Application to north sea illite-tobellite-smectite-vermiculite. *Clays and Clays*

    Minerals,, **50**, 82-98.

Elie, M., Faure, P., Michels, R., Landais, P. and Griffault, L. (2000) Natural and laboratory oxidation of low-organic-carbon-content sediments: comparaison of chemical changes in hydrocarbons. *Energy and Fuels*, **14**, 854-861.

Espitalié, J., Marquis, F., Sage, L. and Barsony, I. (1987) Géochimie organique du Bassin de Paris. *Revue de l'Institut Français du Pétrole*, **42**, 271-302.

Howard, S.A., and Preston, K.D. (1989) Profile fitting of powder diffraction patterns. Pp. 217-275 in: *Modern Powder Diffraction* (D.L. Bish and J.E. Post, editors). Mineralogical Society of America, Wahington D.C.

Hower, J. and Mowatt, T. C. (1966) The mineralogy of illites and mixed-layer illite/montmorillonites. *American Mineralogist*, **51**, 825-854.

Hower, J., Eslinger, E. V., Hower, M. E. and Perry, E. A. (1976) Mechanism of burial metamorphism of argillaceous sediment: 1. Mineralogical and chemical evidence. *Geological Society of America Bulletin*, **87**, 725-737.

Huang, W.L., Longo, J.M., and Pevear, D.R. (1993) An experimentally derived kinetic model for smectite-to-illite conversion and its use as a geothermometer. *Clays and Clay Minerals*, **41**, 162-177.

Inoue, A., Bouchet, A., Velde, B. and Meunier, A. (1989) Convenient technique for estimating smectite layer percentage in randomly interstratified illite/smectite minerals. *Clays and Clay Minerals*, **37**, 227-234.

Landais, P. and Elie, M. (1999) *Utilisation de la géochimie organique pour la détermination du paléoenvironnement et de la paléothermicité dans le Callovo-Oxfordien du site de l´Est de la france. Etude de l´Est du bassin de Paris*, Edition EDP Sciences, 35-61.

Lanson, B. (1990) Mise en évidence des mécanismes de transformation des interstratifiés illite/smectite au cours de la diagenèse. Ph.D. thesis, Université Paris 6 - Jussieu, France, 366 pp.

Lanson, B. and Champion, D. (1991) The I/S-to-illite reaction in the late stage diagenesis. *American Journal of Science*, **291**, 473-506.

Lanson, B. and Besson, G. (1992) Characterization of the end of smectite-to-illite transformation: Decomposition of X-ray patterns. *Clays and Clay Minerals*, **40**, 40-52.

Lindgreen, H., Drits, V.A., Sakharov, B.A., Salyn, A.L., Wrang, P. and Dainyak, L. (2000) Illite-smectite structural changes during metamorphism in black Cambrian Alum shales from the Baltic area. *American Mineralogist*, **85**, 1223-1238.

de Marsily, G., Goncalves, J., Violette, S. and Castro, M.C. (2002) Migration mechanisms of radionuclides from a clay repository toward adjacent aquifers and the surface. *Comptes Rendus Physique*, **3**, 945-959.

Meunier, A. and Velde, B. (1989) Solid solutions in I/S mixed-layer minerals and illite. *American Mineralogist*, **74**, 1106-1112.

Meunier, A., Lanson, B. and Beaufort, D. (2000) Vermiculitization of smectite interfaces and illite layer growth as a possible dual model for illite-smectite illitization in diagenetic environments: a synthesis. *Clay Minerals*, **35**, 573-586.

Meunier A. and Velde B. (2004) *Illite. Origins, evolution and metamorphism*. Springer-Verlag, Berlin, in press.

Meunier A., Lanson B. and Velde B., (2004) Composition variation of illite-vermiculite-smectite mixed-layer minerals in a bentonite bed from Charente (France), *Clay Minerals*, **39**, in press.

Moore, D. M. and Reynolds, R. C., Jr (1989). *X-ray Diffraction and the Identification and Analysis of Clay Minerals*. Oxford University Press, Oxford and New York, 322 pp.

Pellenard, P., Deconinck, J. F., Marchand, D., Thierry, J., Fortwengler, D. and Vigneron, G. (1999) Eustatic and volcanic influenc during Middle Callovian Oxfordian clay

sedimentation in the eastern part of the Paris Basin. *Compte rendus de l´academie des sciences*, **328**, 807-813.

Perry, E. A., Jr and Hower, J. (1970) Burial diagenesis in Gulf Coast pelitic sediments. *Clays and Clay Minerals*, **18**, 165-177.

Pytte, A. M. and Reynolds, R. C. (1989) The thermal transformation of smectite to illite. Pp. 133-140 in: *The thermal history of sedimentary basin : methods and case histo*ry (N. D Naesser and T. H MCCulloh, editors). Springer-Verlag, New York.

Righi, D., Velde, B. and Meunier A. (1995) Clay stability in clay-saturated soil systems. *Clay Minerals*, **30**, 45-54.

Rousset, D. and Clauer, N. (2003) Discrete clay diagenesis in a very low-permeable sequence constrained by an isotopic (K-Ar and Rb-Sr) study. *Contributions to Mineralogy and Petrology*, **145**, 182-198.

Sakharov, B. A., Lindgreen, H., Salyn, A. and Drits, V. (1999) Determination of illite-smectite structures using multispecimen XRD profile fitting. *Clays and Clays Minerals*, **47**, 555-566.

Sato, T., Murakami, T. and Watanabe, T. (1996) Change in layer charge of smectites and smectite layers in illite/smectite during diagenetic alteration. *Clays and Clay Minerals*, **44**, 460-469.

Shutov, V.D., Drits, V.A. and Sakharov, B.A. (1969) On the mechanism of a postsedimentary transformation of montmorillonite into hydromica. Pp. 523-531 in: *Proceedings of the International Clay Conference*, *Tokyo* (L. Heller, editor). Israel University Press, Jerusalem.

Srodon, J. (1978) Correlation between coal and clay diagenesis in the Carboniferous of the upper Silesian coal basin. *Proceedings of the International Clay Conference*, *Oxford*, pp. 251-260.

Srodon, J. (1980) Precise identification of illite/smectite interstratifications by X-ray powder diffraction. *Clays and Clay Minerals*, **28**, 401-411.

Srodon, J. (1981) X-Ray identification of randomly interstratified illite-smectite in mixtures with discrete illite. *Clay Minerals*, **16**, 297-304.

Srodon, J. (1984) Mixed-layer illite-smectite in low-temperature diagenesis: Data from the Miocene of the Carpathian foredeep. *Clay Minerals*, **19**, 205-215.

Srodon, J. and Eberl, D. D. (1984) Illite. Pp. 495-544 in: *Micas* (S. W. Bailey). Reviews in Mineralogy, **13**, Mineralogical Society of America, Washington D.C.

Srodon, J., Elsass, F., McHardy, W. J. and Morgan, D. J. (1992) Chemistry of illite-smectite inferred from TEM measurements of fundamental particles. *Clay Minerals*, **27**, 137-158.

Velde, B. and Peck, T., (2002) Clay mineral changes in the morrow experimental plots, University of Illinois. *Clays and Clay Minerals*, **50**, 364-370.

Velde, B., Suzuki, T. and Nicot, E. (1986) Pressure-Temperature-Composition of illite/smectite mixed-layer minerals: Niger delta mudstones and other examples. *Clays and Clay Minerals*, **34**, 435-441.

Velde, B. and Espitalié, J. (1989) Comparison of kerogen maturation and illite/smectite composition in diagenesis. *Journal of Petroleum Geology*, **12**, 103-110.

Velde, B. and Vasseur, G. (1992) Estimation of the diagenetic smectite to illite transformation in time-temperature space. *American Mineralogist*, **77**, 967-976.

Watanabe, T. (1981) Identification of illite/montmorillonite interstratification by X-ray powder diffraction. *Journal of the Mineralogical Society of Japan*, **Spec. Issue 15**, 32-41.

Watanabe, T. (1988) The structural model of illite/smectite interstratified mineral and the diagram for their identification. *Clay Science*, **7**, 97-114.

Whitney, G. (1990) Role of water in the smectite-to-illite reaction. *Clays and Clay Minerals*, **38**, 343-350.

Whitney, G. (1992) Dioctahedral smectite reactions at elevated temperatures: Effects of K-availability, Na/K ratio and ionic strength. *Applied Clay Science*, **7**, 97-112.

Table 1. Mineralogical characterization of sample 447 using the identification methods proposed by Srodon (1981) and Inoue *et al.* (1989) for the identification of randomly interstratified (R = 0) I-S MLMs.

Identification method	(Srodon, 1981)	(Inoue *et al.,* 1989)
Criterion	Position (15-16°2θ range): 15.94°2θ Position (31-32°2θ range): 31.46°2θ Uncorrected smectite content: 60% $\dfrac{I_I}{I_{I-S}} = 1.63$ Smectite content correction: 15%	$\dfrac{\text{Saddle}}{\text{Peak}}$ ratio : 0.82
%I in the randomly interstratified I-S MLM	25	45
R$_{WP}$ (%)	32.0	19.7

Note: R$_{WP}$ is the usual criterion to assess the quality of fit. This value has been calculated after simulation of the I-S contribution according to the identification performed. Other contributions to the diffracted intensity from discrete illite, kaolinite, and chlorite were introduced as in the optimum fit (Tables 2a-d). The R$_{WP}$ value obtained for the structural model proposed for sample 447 (Ca-EG) is 8.8%.

Table 2a. Composition of the smectite phase throughout the Callovo-Oxfordian series in the EST 104 borehole (Group 1 samples). Structural parameters are determined from XRD profile fitting using the multi-specimen technique (Sakharov *et al.,* 1999).

Sample	State Layer type	Ca-EG S	Ca-EG V	Ca-AD S	Ca-AD V
	L. Tck. (Å)	16.7	12.9	15.0	12.5
447	Rel. Prop. (%)	100	0	60	40
482	Rel. Prop. (%)	100	0	70	30
489	Rel. Prop. (%)	100	0	60	40
492	Rel. Prop. (%)	100	0	70	30
494	Rel. Prop. (%)	100	0	75	25

Note: L. Tck. is the basal spacing along the c* axis of the different layer types present in the smectite phase. S and V layer types are differentiated from their swelling behaviors. S layers incorporate 2 sheets of ethylene glycol (EG) after EG solvation (Ca-EG) and/or 2 sheets of water molecules in the air dried state (Ca-AD). In these states, V layers incorporate 1 sheet of EG molecules and/or 1 sheet of water molecules, respectively. Rel. Prop. is the relative proportion of each layer type in the smectite crystallites. For all samples the mean coherent scattering domain size (CSDS) along the c* axis is 3.5 layers in the AD state and 3.0 in the EG state (lognormal distribution).

Table 2b. Composition of the I-Exp MLM (R=0) phase throughout the Callovo-Oxfordian series in the EST 104 borehole (Group 1 samples). Structural parameters are determined from XRD profile fitting using the multi-specimen technique (Sakharov *et al.,* 1999).

Sample	State Layer type	Ca-EG I	S	V	Ca-AD I	S	V
	L. Tck. (Å)	9.98	17.0	12.9	9.98	15.0	12.5
447	Rel. Prop.	65	25	10	65	20	15
482	Rel. Prop.	65	25	10	65	25	10
489	Rel. Prop.	65	25	10	65	20	15
492	Rel. Prop.	65	25	10	65	22	13
494	Rel. Prop.	65	28	7	65	20	15

Note: All notations as for Table 2a. I denotes non-expandable (illite) layers. For all samples the mean CSDS along the c^* axis is 12 layers in both AD and EG states (lognormal distribution).

Table 2c. Composition of the I-Exp mixed-layer phases for sample 528. Structural parameters are determined from XRD profile fitting using the multi-specimen technique (Sakharov *et al.,* 1999).

	MLM1 (R = 0)				
	Ca-EG		Ca-AD		
L. Tck. (Å)	9.98	16.8	9.98	15	12.5
Rel. Prop. (%)	70	30	70	20	10

	MLM2 (R = 1)					
	Ca-EG			Ca-AD		
	I	S	V	I	S	V1	V2
L. Tck. (Å)	9.98	16.8	13.5	9.98	15.0	12.5	12.5
Rel. Prop.	70	15	15	70	5	10	15

Junction probability parameters (Ca-EG):
$P_{SS} = 0.15$, $P_{SV} = 0.15$
$P_{VS} = 0.15$, $P_{VV} = 0.40$

Junction probability parameters (Ca-AD):
$P_{SS} = 0.05$, $P_{SV1} = 0.10$, $P_{SV2} = 0.15$
$P_{V1S} = 0.05$, $P_{V1V1} = 0.10$, $P_{V1V2} = 0.15$
$P_{V2S} = 0.05$, $P_{V2V1} = 0.10$, $P_{V2V2} = 0.40$

	I	S1	S2	V
L. Tck. (Å)	9.98	15.0	15.0	12.5
Rel. Prop.	70	15	5	10

Junction probability parameters:
$P_{S1S1} = 0.15$, $P_{S1S2} = 0.05$, $P_{S1V} = 0.10$
$P_{S2S1} = 0.15$, $P_{S2S2} = 0.13$, $P_{S2V} = 0.27$
$P_{VS1} = 0.15$, $P_{VS2} = 0.13$, $P_{VV} = 0.27$

Note : All notations as for Table 2a. Relative abundance of MLM1 is 23% and 20% in EG and AD states, respectively. Relative abundance of MLM2 is 45% and 48% (15% + 33%) in EG and AD states, respectively. The mean CSDS along the c* axis is 12 layers in both AD and EG states (lognormal distribution)

Table 2d. Relative proportions of the different phases contributing to the diffracted intensity in the sampled Callovo-Oxfordian series (EST 104 borehole) as determined from XRD profile fitting using the multi-specimen technique (Sakharov *et al.,* 1999).

Sample	State	I-Exp MLM (%)	Smectite (%)	Illite (%)	Kaolinite (%)	Chlorite (%)	R_{WP} (%)
447	Ca-EG	54	24	21	0	1	8.8
	Ca-AD	55	20	25	0	1	11.5
482	Ca-EG	54	20	25	0	1	7.7
	Ca-AD	53	18	28	0	1	9.7
489	Ca-EG	67	10	21	0	2	10.5
	Ca-AD	62	10	27	0	1	11.0
492	Ca-EG	66	4	24	5	1	10.1
	Ca-AD	61	4	29	5	1	10.6
494	Ca-EG	68	1	27	3	1	8.0
	Ca-AD	66	3	27	3	1	10.8
528	Ca-EG	68[*]	0	21	10	1	12.2
	Ca-AD	68[*]	0	21	10	1	13.2

Note : Relative proportions are given as weight %. [*] For sample 528 the contributions of both MLM1 and MLM2 (Table 2c) are summed up to determine the relative contribution of the I-Exp MLM phase. R_{WP} is the usual parameter to assess the quality of fit.

FIGURE CAPTION

Figure1. Sample location. MHM indicates the planned Meuse / Haute-Marne underground laboratory. Boreholes EST 104 and EST 204 are located nearby. GSY, CPG, MRY, CPY,CEY, MOP, BAT, CHV are boreholes drilled for oil exploration purposes (Lanson, 1990).

Figure 2. Experimental XRD patterns (oriented slides, <0.2 µm size fraction) of the six samples selected as being representative of the Callovo-Oxfordian series (Claret, 2001). Group 1 (Gp1) samples exhibit a 17.3 Å peak in the EG state, whereas sample 528 does not show this diffraction maximum. The solid and gray traces represent XRD patterns recorded in AD state and after EG salvation respectively. Peak positions are outlined as dashed lines for mica (M), chlorite (Ch), and quartz (qz) contributions. Peak positions of other clay minerals are outlined as dot-dashed and solid lines for AD and EG states, respectively.

Figure 3. Comparison of experimental XRD patterns characteristic of group 1 (Gp1, sample 447) and sample 528 with that obtained (**a**) on Oxfordian samples from borehole EST 204 (MHM 218-249) (oriented slides, <2 µm size fraction)and (**b**) on samples from Toarcian black shales taken at various burial depth throughout the Paris basin (Lanson, 1990-oriented slides, <2 µm size fraction). Patterns and peak positions as in Figure 2.

Figure 4. elementary contributions to the diffracted intensity as determined using the multi-specimen method developed by Sakharov *et al.* (1999) to the XRD pattern recorded on sample 447. Experimental XRD patterns are shown as crosses, whereas the respective contribution of discrete smectite, I-Exp MLM, and illite are shown from top to bottom as

solid, dashed, and dot-dashed lines, respectively. Relative intensities of these elementary contributions are normalized according to their relative proportions (Table 2d). Positions of the diffraction maxima are indexed, and quartz (qz) impurity is labeled. The broken x-axis indicates a scale change. (**a**) Ca-saturation and EG solvation. Scale factor x5 over the 14-50°2θ CuKα range. (**b**) Ca-saturation and AD state. Scale factor x10 over the 14-50°2θ CuKα range.

Figure 5. Comparison between experimental and calculated XRD patterns for sample 447. Experimental data are shown as crosses, whereas the optimum fit is shown as a solid line. Structural parameters leading to the optimum fit presented are given in Table 2. Positions of the diffraction maxima are indexed, and quartz (qz) impurity is labeled. The gray rectangle indicates a scale change. (**a**) Ca-saturation and EG solvation. Scale factor x6.5 over the 14-50°2θ CuKα range. (**b**) Ca-saturation and AD state. Scale factor x10 over the 14-50°2θ CuKα range.

Figure 6. Comparison between experimental and calculated XRD patterns for sample 492. Structural parameters leading to the optimum fit presented are given in Table 2. Patterns as for Figure 5. (**a**) Ca-saturation and EG solvation. Scale factor x3 over the 14-50°2θ CuKα range. (**b**) Ca-saturation and AD state. Scale factor x5 over the 14-50°2θ CuKα range.

Figure 7. Comparison between experimental and calculated XRD patterns for sample 528. Structural parameters leading to the optimum fit presented are given in Table 2. Patterns as for Figure 5. (**a**) Ca-saturation and EG solvation. Scale factor x3 over the 14-50°2θ

CuKα range. (**b**) Ca-saturation and AD state. Scale factor x6.5 over the 14-50°2θ CuKα range.
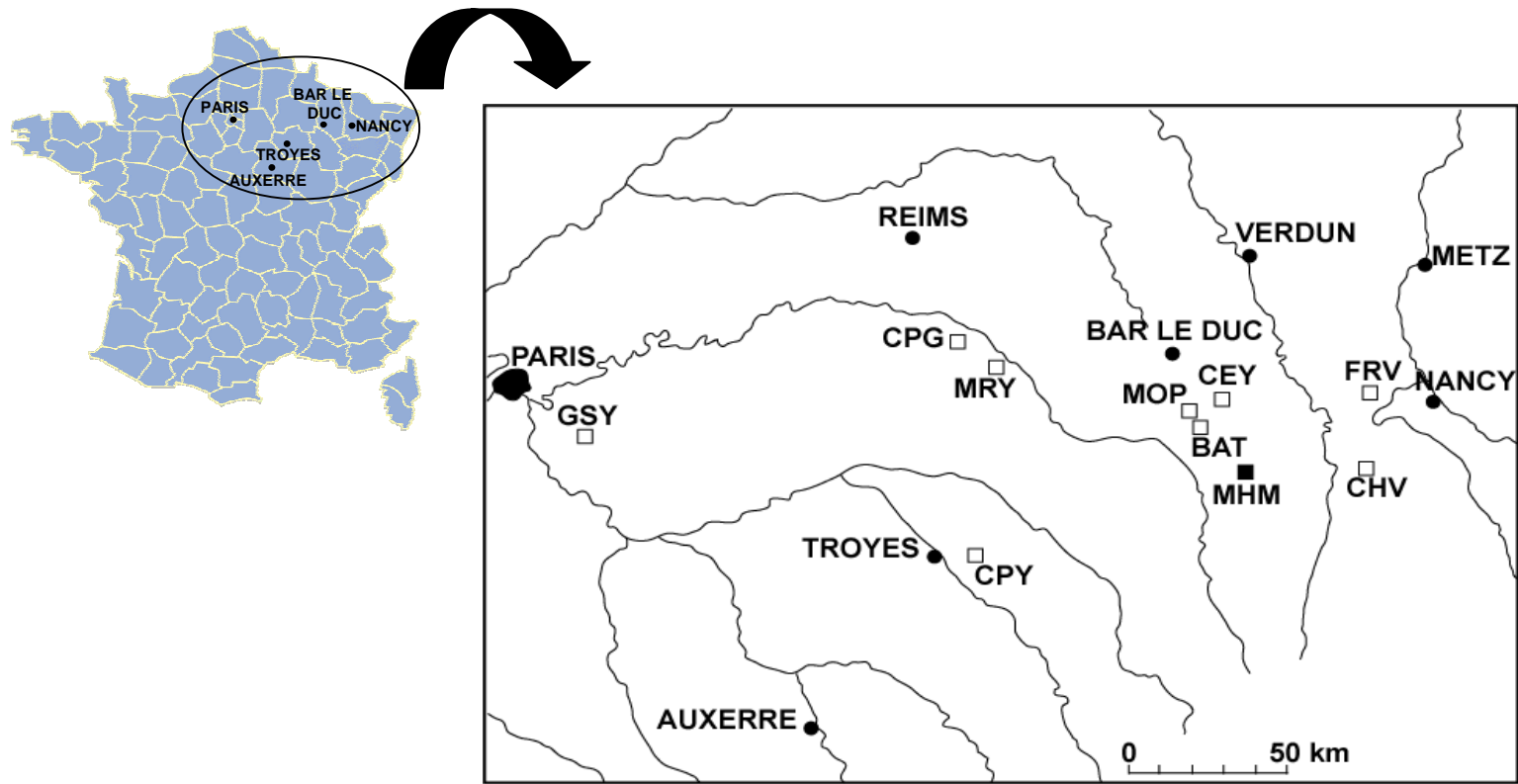
Figure 8. Comparison between the occurrence probability of the different layer pairs in an I-S-V MLM calculated for different structure models. Solid bars represent the randomly interstratified (R = 0) I-Exp MLM phase (65 %I, 25 %S, 10 %V) used to describe samples from group 1 in the Ca-EG state. Open bars represent the combined contribution of MLM1 and MLM2 phases used to describe sample 528 in the Ca-EG state. MLM1 and MLM2 contributions were calculated separately and summed up using their optimum ratio (23:45 – Table 2c). Hatched bars represent a randomly interstratified (R = 0) I-Exp MLM phase with the same composition (70 %I, 20 %S, and 10 %V) as the combined contribution of MLM1 and MLM2 used to describe sample 528 in the Ca-EG state.

Figure 9. Sensitivity of the trial-and-error calculation procedure used in the multi-specimen method to structural parameters. Patterns as for Figure 5. Arrows indicate significant misfit as compared to the optimum fits shown in Figures 5-7. Structural parameters for the optimal models are given in Table 2. (**a**) Sample 447 Ca-saturated after EG solvation. V layers in the I-Exp MLM are replaced by S layers leading to a 65:35:0 I:S:V ratio in this phase as compared to the optimum 65:25:10 ratio (Table 2b. Scale factor x6.5 over the 14-50°2θ CuKα range. (**b**) Sample 447 Ca-saturated after EG solvation. S layers are slightly segregated in the I-Exp MLM as P_{SS} is increased from the optimum 0.25 value ($P_{SS} = W_S$ as R = 0) to 0.40 ($P_{SS} > W_S$). Scale factor x6.5 over the 14-50°2θ CuKα range. (**c**) Sample 447 Ca-saturated after EG solvation. The basal distance of S layers along the c* axis is increased from the optimum 17.0 Å value to 16.7 Å. Optimum fit is shown as a solid line whereas the alternative model leads to the dashed line. Scale factor x6.5 over
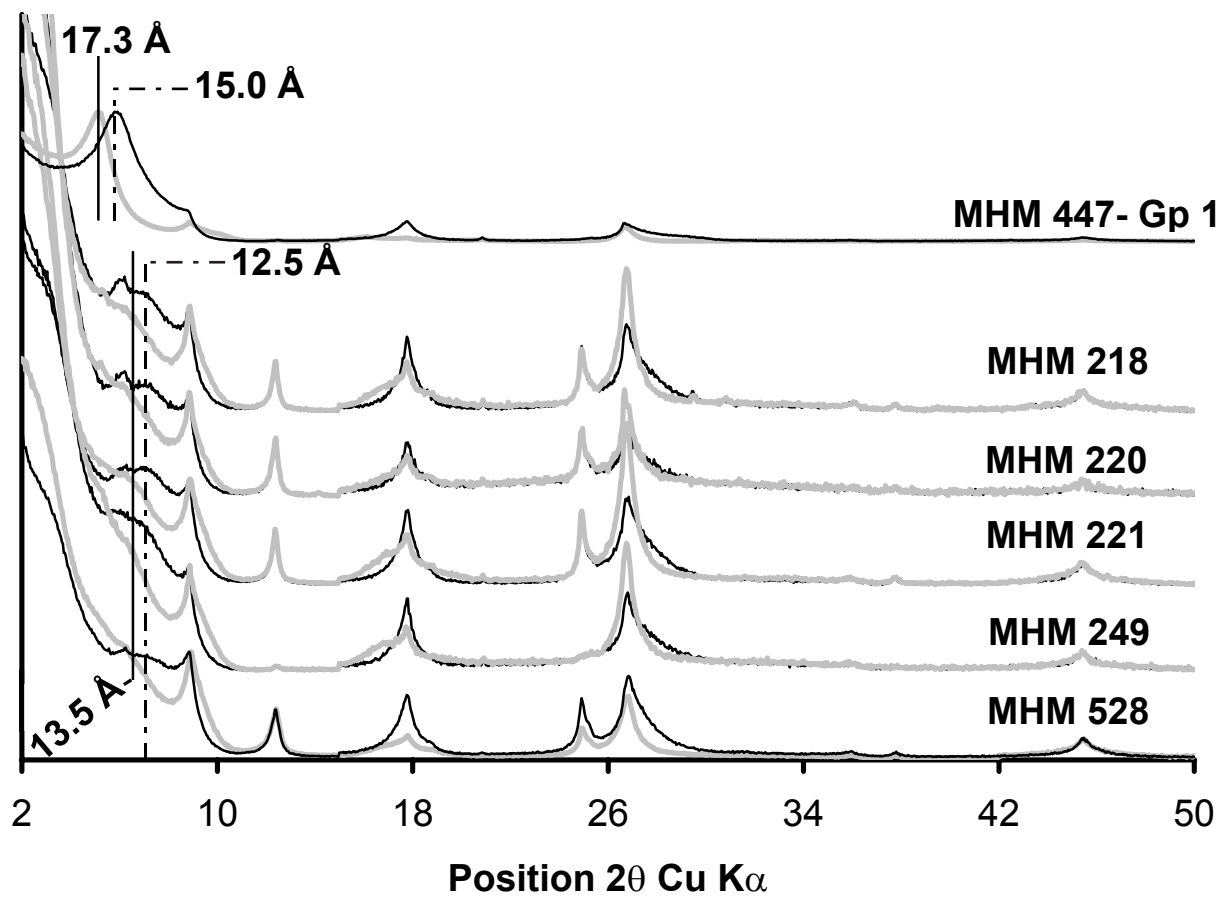
the 14-50°2θ CuKα range. (**d**) Sample 492 Ca-saturated after EG solvation. The K-content of I layers in the I-Exp MLM is increased from the optimum 0.75 value to 0.90 (K per $O_{10}(OH)_2$). Scale factor x3 over the 14-50°2θ CuKα range.
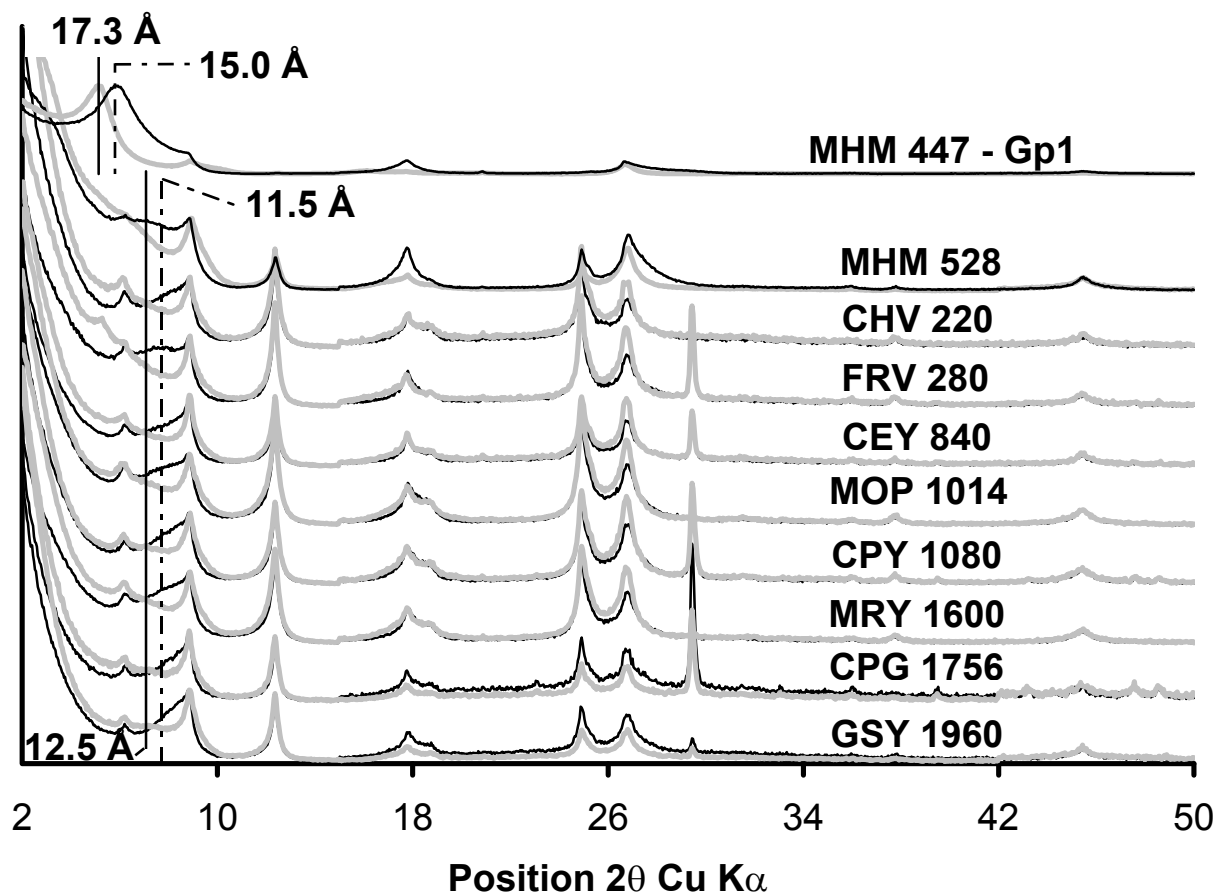
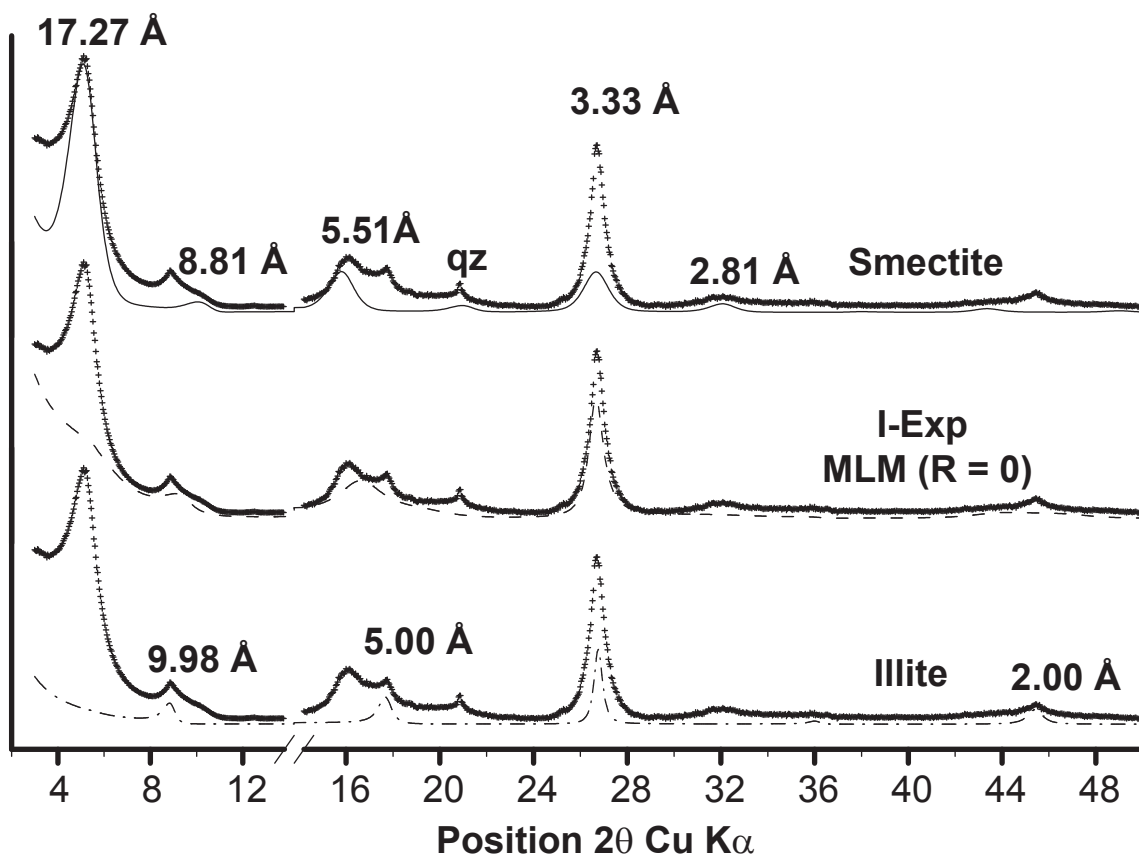**Figure 10**. TEM micrographs obtained on the <0.05 µm fraction after Na-saturation. Assemblages of lath-shaped particles (I-Exp MLMs) with relative orientations of 120° may be observed throughout the whole Callovo-Oxfordian series.
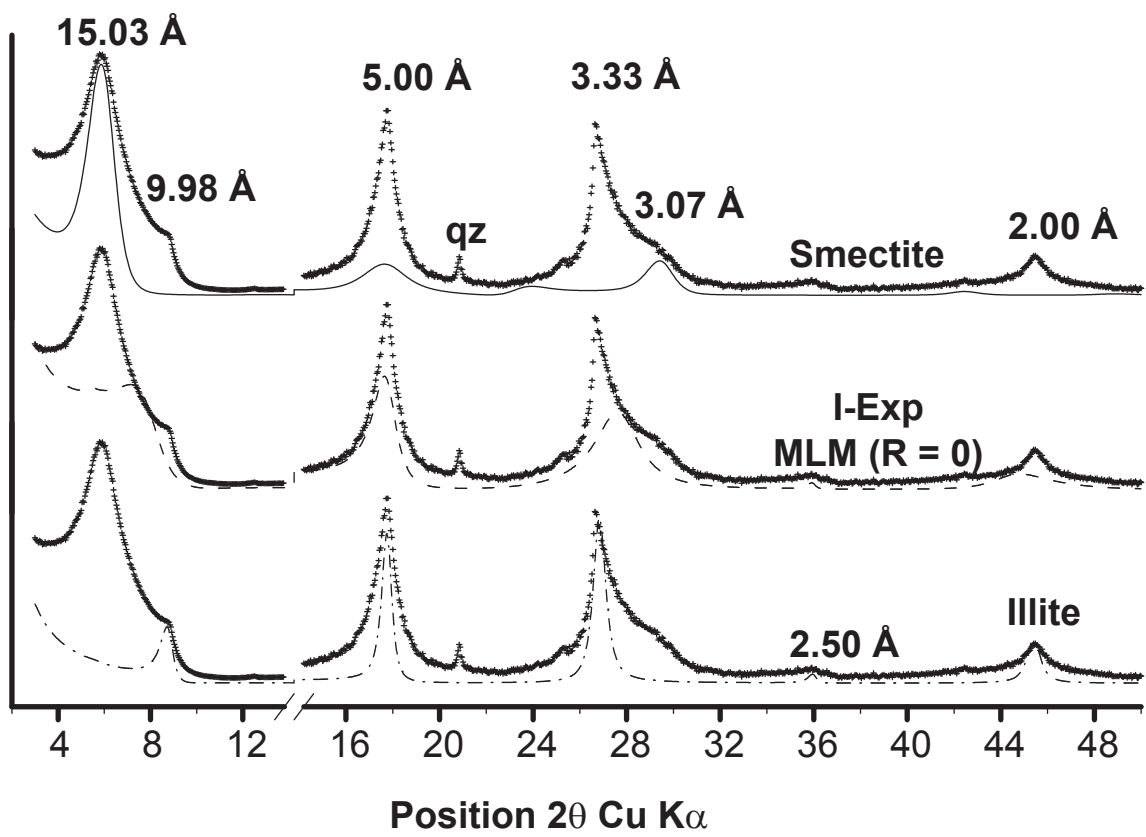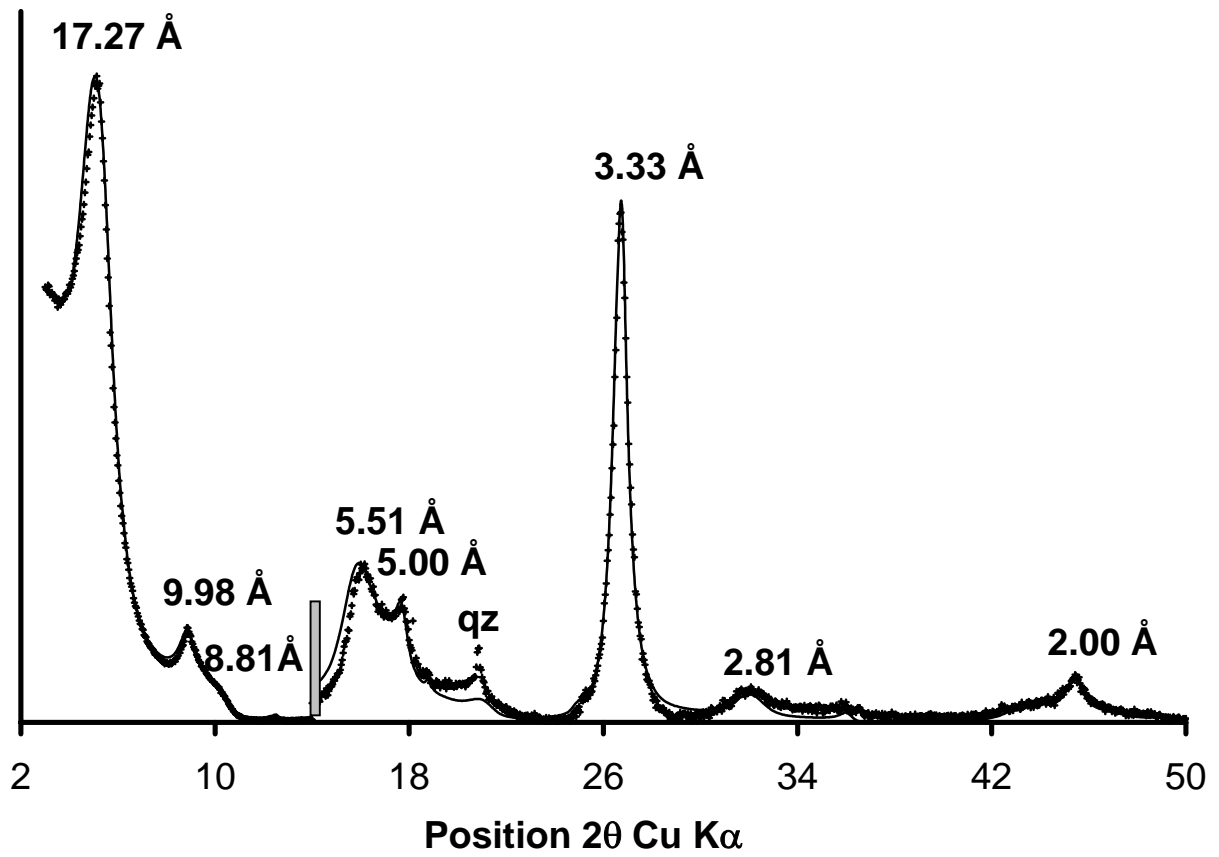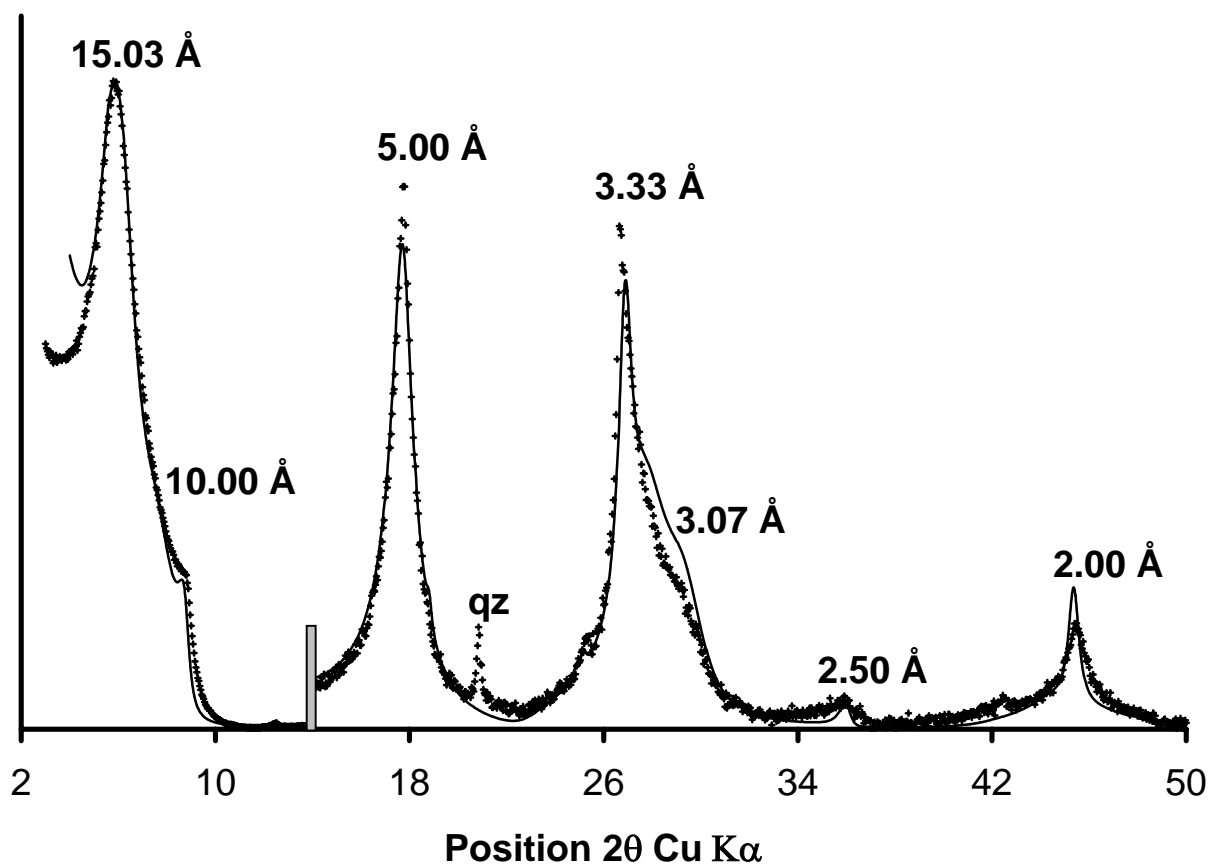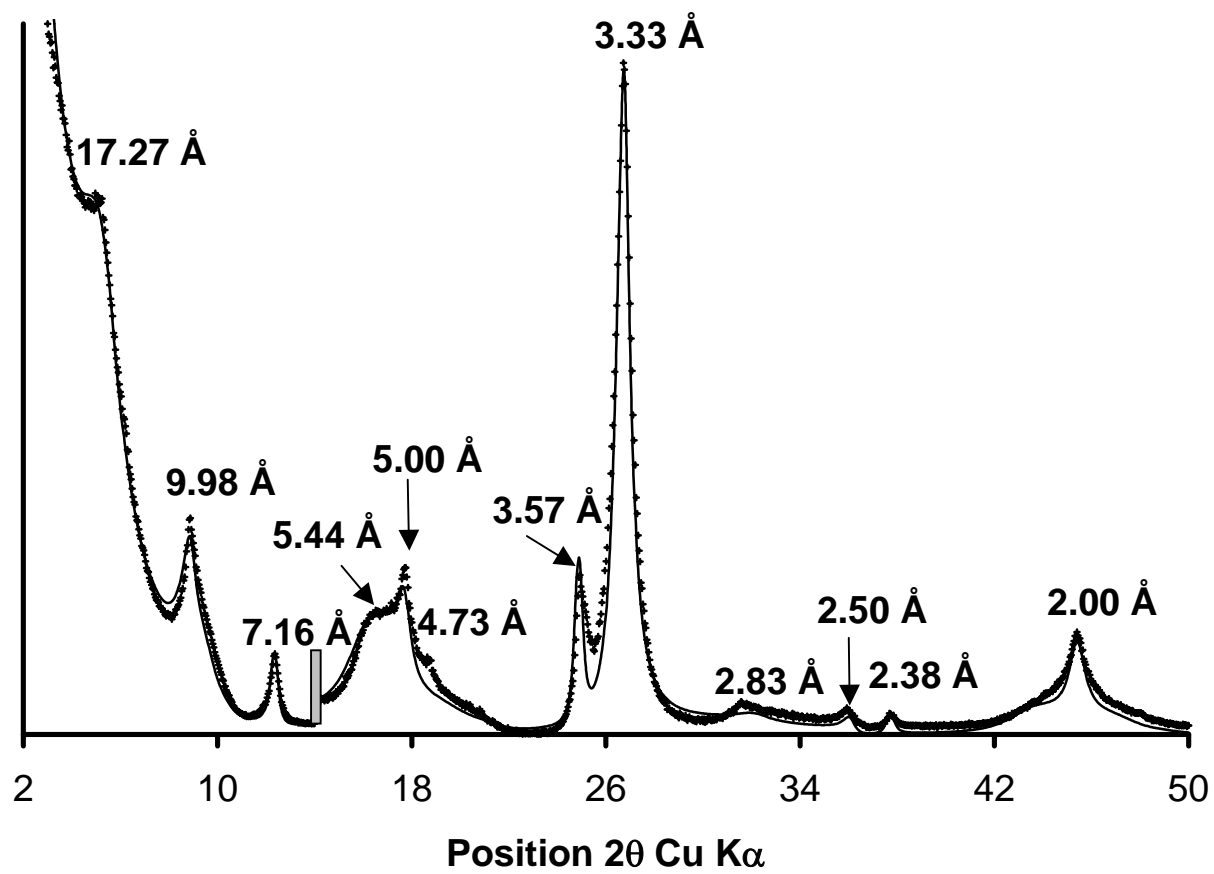
PARIS
BAR LE
DUC
NANCY
TROYES
AUXERRE

REIMS
VERDUN
METZ
PARIS
CPG
BAR LE DUC
CEY
FRV
NANCY
GSY
MRY
MOP
BAT
CHV
MHM
TROYES
CPY
AUXERRE

0   50 km

Claret et al., Figure1

17.3 Å

15.0 Å

M **Ch** **M** **Ch**

M **Ch** **M+I/S+Qz** **M**

- 447 m

- 482 m

Gp 1

- 489 m

Kaolinite | Onset

- 492 m

13.5 Å **12.5 Å**

- 494 m

- 528 m

2   10   18   26   34   42   50

Position 2θ Cu Kα

Claret et al., Figure 2

17.3 Å

15.0 Å

MHM 447- Gp 1

12.5 Å

MHM 218

MHM 220

MHM 221

MHM 249

13.5 Å

MHM 528

Position 2θ Cu Kα

Claret et al., Figure 3a

17.3 Å

15.0 Å

11.5 Å

MHM 447 - Gp1

MHM 528

CHV 220

FRV 280

CEY 840

MOP 1014

CPY 1080

MRY 1600

CPG 1756

GSY 1960

12.5 Å

Position 2θ Cu Kα

Claret et al., Figure 3b

17.27 Å

3.33 Å

8.81 Å

5.51Å

qz

2.81 Å   Smectite

I-Exp
MLM (R = 0)

9.98 Å

5.00 Å

Illite   2.00 Å

Position 2θ Cu Kα

4   8   12   16   20   24   28   32   36   40   44   48

Claret et al, Fig 4a

15.03 Å

5.00 Å

3.33 Å

9.98 Å

3.07 Å

qz

2.00 Å

Smectite

I-Exp
MLM (R = 0)

2.50 Å

Illite

Position 2θ Cu Kα

Claret et al, Fig 4b

Claret et al., Figure 5a

15.03 Å

5.00 Å

3.33 Å

10.00 Å

3.07 Å

2.00 Å

qz

2.50 Å

Position 2θ Cu Κα

Claret et al., Figure 5b

17.27 Å

3.33 Å

9.98 Å

5.00 Å

5.44 Å

3.57 Å

7.16 Å

4.73 Å

2.50 Å

2.00 Å

2.83 Å

2.38 Å

Position 2θ Cu Kα

2   10   18   26   34   42   50

Claret et al., Figure 6a

Claret et al., Figure 6b

14.21 Å

9.98 Å

7.16 Å

5.00 Å

4.73 Å

3.57 Å

3.33 Å

2.83 Å

2.50 Å

2.38 Å

2.00 Å

Position 2θ Cu Kα

2   10   18   26   34   42   50

Claret et al., Figure 7b

Claret et al., Figure 8

17.27 Å

3.33 Å

5.00 Å

9.98 Å

qz

2.81 Å

2.00 Å

Position 2θ Cu Kα

Claret et al., Figure 9a

17.27 Å

3.33 Å

5.51 Å

9.98 Å

qz

2.81 Å

2.00 Å

Position 2θ Cu Kα

Claret et al., Figure 9b

3.32 Å

3.34 Å

Position 2θ Cu Kα

Claret et al., Figure 9c

17.27 Å

9.98 Å

5.00 Å

3.33 Å

2.00 Å

Position 2θ Cu Kα

Claret et al., Figure 9d

- 447 m

- 489 m

- 528 m

120°

Claret et al., Figure 10